PHYSICAL REVIEW B VOLUME 23, NUMBER 7 1 APRIL 1981

Raman scattering from superconducting gap excitations in the presence of a magnetic field

R. Sooryakumar* and M. V. Klein
Department of Physics and Materials Research Laboratory, University of Illinois, Urbana, Illinois 61801
(Received 3 October 1980)

We recently observed, using Raman scattering as a probe, the superconducting gap excitation in $2H$-$NbSe_2$. This was seen by the appearance of two new Raman-active modes of different symmetry A (18 cm^{-1}) and E (15 cm^{-1}) when the sample is superconducting. In this paper we present further experimental details and results that confirm the theory of Balseiro and Falicov, which shows that the new modes borrow their Raman activity from low-lying charge-density-wave (CDW) phonons. Evidence of this direct coupling between superconducting electrons and the CDW phonon is seen by the behavior of the modes in a magnetic field. Such behavior of the Raman spectra is explained in terms of a model involving a complex gap. The effect of lifetime broadening of the CDW phonon and consequences of varying coupling strength are presented.

Our recently published[1] experimental results and the theoretical calculations[2] of Balseiro and Falicov on Raman scattering from the superconductor $2H$-$NbSe_2$ highlight the importance of coupling between superconducting electrons and the charge-density-wave (CDW) phonon. The superconducting properties are observed by the appearance of new Raman-active modes of different symmetries A (18 cm^{-1}) and E (15 cm^{-1}) when the sample is immersed in superfluid helium. The Raman spectra from $2H$-$NbSe_2$ with varying impurity contents presented in Ref. 3, showed experimentally, among other results, the necessity of having a low-lying Raman-active phonon to couple the incident light to the superconducting electrons. In this paper we present experimetal details and further magnetic field data that clearly demonstrate the coupling between the new peaks and the CDW phonon. The behavior of the Raman spectra in an external field is explained qualitatively in terms of a simple model involving a complex gap parameter. The effect of lifetime broadening of the CDW phonon and consequences of varying the coupling strength are discussed.

I. EXPERIMENTAL DETAILS

It has been estimated[4] that laser heating in the transition metal dichalcogenides is approximately 40 K for 100 mW power. In order to ensure that $2H$-$NbSe_2$ is below its superconducting transition temperature T_c of 7 K, 30 mW of incident power is spread (and not focused to a spot) on the sample which is immersed in superfluid helium. Cooling the sample by flowing cold helium gas is insufficient to maintain it superconducting. Due to experimental restrictions, we were able to vary the temperature by only 0.5 K, between 1.6 and 2.1 K and still ensure a local sample temperature less than T_c. In this limited temperature range the value of the energy gap should change by about 4%, i.e., a $\frac{1}{2}$-cm^{-1} shift in 2Δ. Experimentally we could not observe any change in the peak position within this 0.5-K range. The only other "convenient" technique available to vary the BCS gap and hence to confirm the involvement of superconductivity with the new peaks was to apply a magnetic field.

The magnetic field dependent data were obtained using a split-coil superconducting magnet from American Magnetics Incorporated (AMI No. 10236). Owing to the rapid quenching of the gap modes, the maximum field of 42 kG produced by this system was adequate. However, one of the main drawbacks of the system was that it could be operated only at 2 K. The magnet coil assembly and sample were in the same chamber of the cryostat. Having to maintain the magnet coil in liquid helium forced the sample to also be at this temperature. The diameter of the magnet bore was 0.5 in. This resulted in an effective solid angle which was about half of that obtained without the magnet coil. Hence, the signal-to-noise ratio for runs done with the magnet were smaller than that from standard Janis cryostats.

The runs with the magnetic field were conducted with the sample in two orientations. In one orientation, the sample layers were parallel to the magnetic field and in the other they were perpendicular. The parallel orientation had the sample at the end of an insert with its layers vertical. The scattered light was collected along the c axis. The case with the layers perpendicular to the field is more tricky. The layers are now horizontal. The inelastically scattered beam

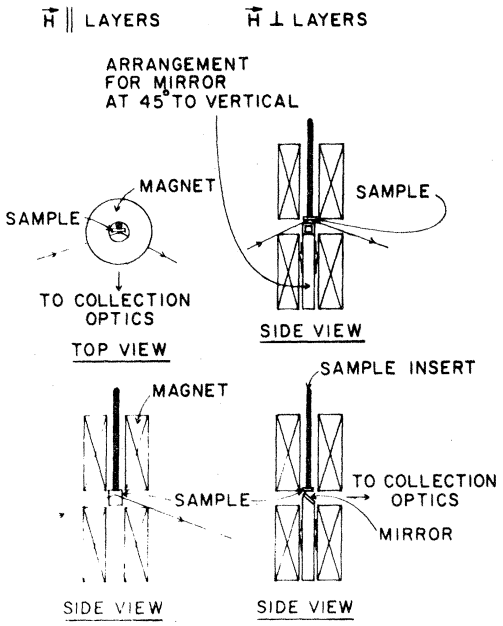

FIG. 1. Position of sample with respect to magnet for magnetic fields parallel and perpendicular to layers.

is again collected along the c axis. In order to get this signal to the monochromator, a mirror at 45° to the vertical is placed in the center of the magnet bore. The two orientations of the sample are illustrated in Fig. 1. The mirror which is used to reflect the signal is glued to a Teflon tube which has one edge sliced at 45°. Two small spring clamps are fastened to the side of the Teflon tube to ensure the mirror stays in position when the cryostat is cold. The strength of the magnetic field at the center of the bore is determined from the value of the charging current.

A typical Raman run in either of these configurations was made up as follows: The run was started at about 8 cm^{-1} with 0.5-cm^{-1} steps and 30-sec dwell time. The resolution was 3 cm^{-1}. (XX) and (XY) polarization spectra were taken with the aid of the Polaroid rotator. After scanning through to about 60 cm^{-1}, the monochromator was advanced to 220 cm^{-1}. One wave-number steps at 20 sec/point were then used to scan through the A phonon used for normalization. The digitized data were then used to obtain the spectra on the computer. All runs were normalized with respect to the phonon at 234 cm^{-1}. A five-point computer smoothing was carried out for all curves.

II. MAGNETIC FIELD RESULTS

The data with a magnetic field were taken on sample B.[5] The upper critical fields may be estimated from published data[6] and were found to be 105 and 40 kG at $T=2.50$ K for fields parallel and perpendicular to the layers, respectively. For $2H$-$NbSe_2$, H_{c1}, is a few hundred gauss.[6]

Figures 2–5 show the results obtained for A and E symmetries and different sample orientations with respect to the magnetic field. All curves have been normalized with respect to the energy of the A_{1g} phonon at 234 cm^{-1}.

The A spectrum in Fig. 2 has two features. A CDW-induced mode at about 36 cm^{-1} and the gap peak at 18 cm^{-1}. As H increases the latter loses strength while the CDW mode is seen to recover. It is difficult to assign any movement to the position of the 18-cm^{-1} mode. The new A mode seems to be completely suppressed by a magnetic field of about 14 kG in this configuration, i.e., a third of the upper critical field of 42 kG at this temperature. This figure does clearly show that the new peak is strongly affected by a magnetic field. Furthermore, its Raman activity is seen to be coupled to that of the CDW mode.

We find that the quantity

$$S=\int_0^\infty I(\omega)\,\omega\,d\omega$$

is a constant to within ±7% when H varies over the range in Fig. 2. Here $I(\omega)$ is the number of counts at freqeuncy ω after a common background for all curves has been removed. If there were direct Raman coupling to the gap excitations, there would be a magnetic field-dependent contribution to S. On the other hand, if the only Raman coupling were to the

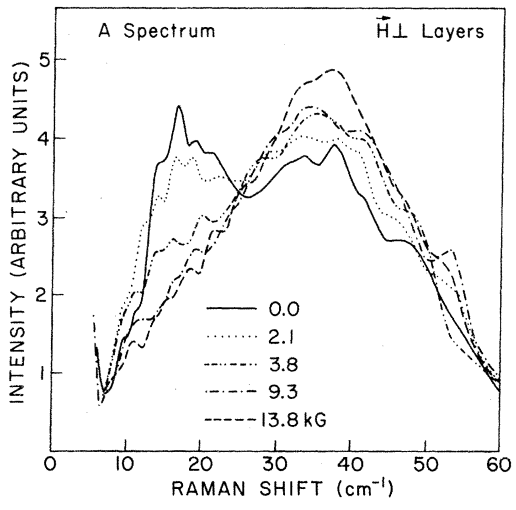

FIG. 2. A-symmetry Raman spectra from sample B carried out with magnetic field perpendicular to layers. The curves represent a 5-point computer smoothing of the data. All curves have been normalized with respect to the A_{1g} phonon at 234 cm^{-1}.

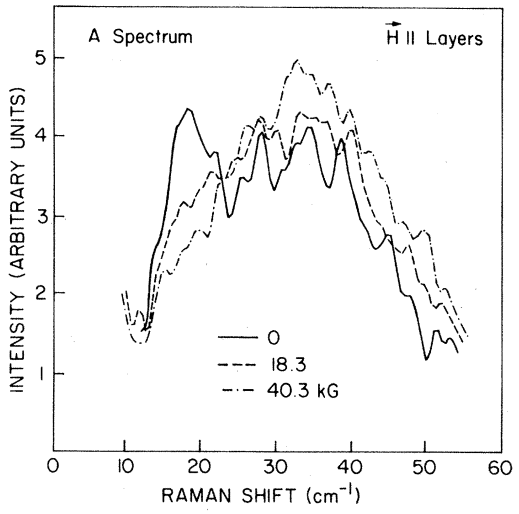

FIG. 3. *A*-symmetry Raman spectra from sample *B* carried out with magnetic field parallel to layers. The curves represent a 5-point computer smoothing of the data. All curves have been normalized with respect to the A_{1g} phonon at 234 cm^{-1}.

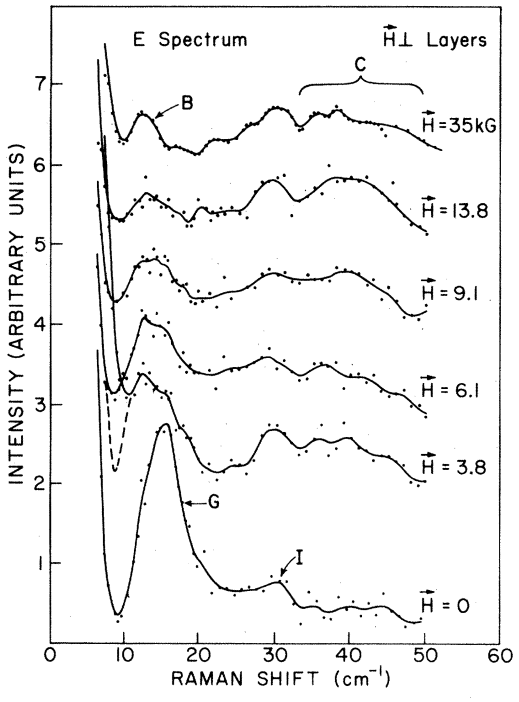

FIG. 4. *E*-symmetry Raman spectra from sample *B* carried out with magnetic field perpendicular to layers. The solid curves represent a 5-point computer smoothing of the data. The dashed line takes account of the larger Rayleigh scattering in that particular run. All curves have been normalized with respect to the A_{1g} phonon at 234 cm^{-1}. *G*: new mode; *C*: CDW-induced mode; *I*: interlayer mode; and *B*: scattering from superfluid helium.

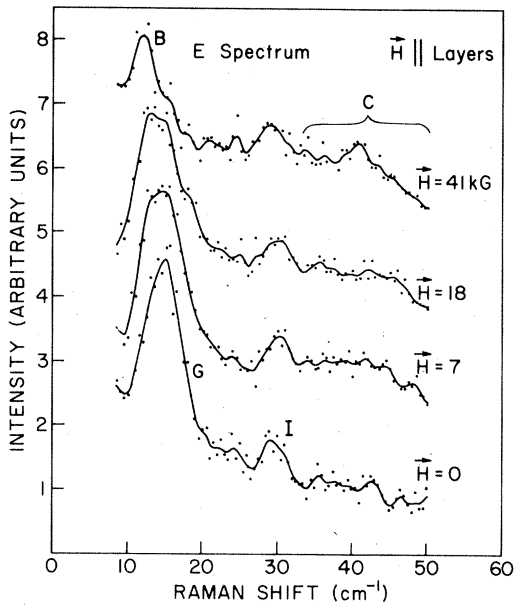

FIG. 5. *E*-symmetry Raman spectra from sample *B* carried out with magnetic field parallel to layers. The solid curve represents a 5-point computer smoothing of the data. All curves have been normalized with respect to the A_{1g} phonon at 234 cm^{-1}. *G*: new mode; *C*: CDW mode; *I*: interlayer mode; and *B*: scattering from superfluid helium.

CDW via a term of the form

$$H'_{\text{eff}} = \chi' u$$

and if the forces acting on the phonon coordinate u were velocity independent then S would be proportional to $|\chi'|^2$, and would be independent of any coupling of phonon coordinate u to other coordinates, including those of the superconducting gap excitations.[7] These are reasonable assumptions; we tentatively conclude that the independence of S from H means that the gap excitations acquire their Raman activity from the CDW phonons.

Figure 3 shows the similar spectrum with sample oriented with its layers parallel to the magnetic field. With a higher crictical field of 105 kG in this orientation we again find that the new peak at 18 cm^{-1} is eliminated by a value of H equal to one third of $H_{c2\|}$.

The *E* spectrum corresponding to $\vec{H}$ being perpendicular to the layers is shown in Fig. 4. The special features of this spectrum have been labeled *B*, *C*, *G*, and *I*. Peak *G* is the new peak induced by superconductivity. As H increases this peak *appears* to soften and its integrated intensity drops. Peak *I* is the "interlayer mode" and is not affected by the superconductivity or the magnetic field. On increasing the fields to higher values we observe a residual peak *B* at (13.4 ± 0.4) cm^{-1}. This is attributed to scattering from superfluid helium. Its position agrees with the helium results of Greytak and Yan.[8] Peak *C* is a

broad CDW induced mode. As H increases, the strength of this peak rises. The width is probably due to inhomogeneous broadening from disorder associated with the incommensurate phase. (The CDW modes of the similar but commensurate structure in $2H$-$TaSe_2$ are much narrower.[9]) Results for H parallel to the layers show the similar effect noted above and are shown in Fig. 5. The peaks B, C, G, and I have the same assignments as for Fig. 4.

Due to the closeness of the 15-cm^{-1} E mode and the 13-cm^{-1} Raman peak from superfluid helium it is necessary to separate these two modes. When $H_\perp$ is large ($\sim$40 kG) the Raman scattering due to superconductivity has been quenched. Hence for this case the scattering for the low ($\lesssim 16$ cm^{-1}) region will be due only to superfluid helium. We subtracted the experimental curve for such a case from all the curves for the E spectra. Figure 6 shows the results for H parallel and perpendicular to the layers. The weak structures I', B' are due to inadequacies in proper subtraction. These occur at frequencies approximately equal to the "interlayer mode" and the second broader helium peak of Ref. 8.

In order to ensure that peak B in Figs. 4 and 5 is due to scattering from superfluid helium, we replaced the sample by a small freshly prepared aluminum mirror and repeated the scan under conditions similar to that used for the actual experiment. We found a peak in the spectrum at an energy corresponding to the position of B. We hence conclude that B is present as a result of scattering from superfluid helium.

This concludes our results on the magnetic field experiments. In summary, our experiments show that the peaks G are strongly affected by rather modest magnetic fields and the Raman activity of these modes is coupled to the CDW modes. It is possible that although the sample is immersed in superfluid helium the sample temperature locally could be greater than 2.1 K due to laser heating. If the inner layers are at a higher temperature, the critical field will be smaller than at 2.1 K. There appears to be no shift in the position of both the A and E peaks G with increasing magnetic field, which was a surprising result. At first thought one would expect the peaks G to soften as the superconductivity is destroyed. Further discussion of these results will be presented later.

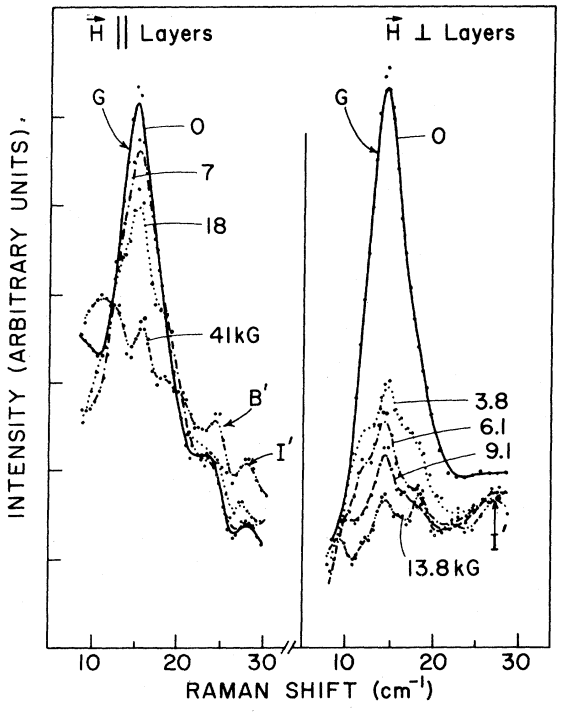

FIG. 6. E-symmetry Raman spectra from sample B with magnetic fields parallel and perpendicular to the layers. These curves are the new modes G after subtracting the helium peak. The curves represent a 5-point computer smoothing. B', I' are a result of inadequacies in the subtraction. These occur at frequencies approximately equal to the superfluid helium peak B' and the interlayer mode.

A. Theory

The Balseiro-Falicov theory[2] explains the origin of the new modes. Their theory states that the new modes at 2 K are a result of interaction between the $q=0$ CDW phonon near 40 cm^{-1} and the superconducting electrons. This indirect coupling of light to the electrons is believed to be the cause of the new peaks. In the presence of electron-phonon interaction, the phonon frequency will be renormalized. The self-energy $\pi(q,\omega)$ approximated by the simplest Feynman diagram for a $q=0$ phonon is given by[10]

$$\pi(0,\omega)=g^2\sum_K \frac{\Delta^2}{\epsilon_K^2}\left[\frac{1}{\omega+2\epsilon_K}-\frac{1}{\omega-2\epsilon_K}\right], \quad (1)$$

where g is the electron-phonon coupling constant, 2Δ the BCS energy gap, and $\epsilon_K^2=\xi_K^2+\Delta^2$, with ξ_K measuring the energy of the system from the Fermi level. In Ref. 2, the bound states λ are calculated via the poles of the renormalized Green's function yielding

$$\lambda^2=\omega_0^2-\frac{16\omega_0\Delta^2 g^2\rho(0)}{\omega(4\Delta^2-\omega^2)^{1/2}}\tan^{-1}\frac{\omega}{(4\Delta^2-\omega^2)^{1/2}},$$

with $\rho(0)$ the density states at the Fermi level and ω_0 the CDW phonon frequency.

B. Lifetime-broadening effects

We have extended these results to include lifetime broadening for the bare phonon. Introducing damping to the phonon Green's function gives

$$D(q\omega)=\frac{2\omega_0}{\omega^2-\omega_0^2-2i\gamma\omega-2\omega_0\pi(q\omega)}. \quad (2)$$

The spectral function $S(q\omega)$ which is the quantity that one measures in a Raman experiment is given at $T=0$ by

$$S(q\omega)=2\,\mathrm{Im}D(q\omega)\ . \tag{3}$$

Thus, for $\omega>2\Delta$ we have

$$S(0\omega)=\frac{4\omega_0\left[2\gamma\omega+\dfrac{8g^2\rho(0)\omega_0\Delta^2\pi}{\omega(\omega^2-4\Delta^2)^{1/2}}\right]}{\left[\omega^2-\omega_0^2-\dfrac{16g^2\rho(0)\Delta^2\omega_0}{\omega(\omega^2-4\Delta^2)^{1/2}}\tanh^{-1}\dfrac{(\omega^2-4\Delta^2)^{1/2}}{\omega}\right]^2+\left[\dfrac{8g^2\rho(0)\Delta^2\omega_0}{\omega(\omega^2-4\Delta^2)^{1/2}}+2\gamma\omega\right]^2}\ , \tag{4}$$

and for $\omega<2\Delta$

$$S(0\omega)=\frac{4\omega_0(2\gamma\omega)}{\left[\omega^2-\omega_0^2+\dfrac{16g^2\rho(0)\Delta^2\omega_0}{\omega(4\Delta^2-\omega^2)^{1/2}}\tan^{-1}\dfrac{\omega}{(4\Delta^2-\omega^2)^{1/2}}\right]^2+(2\gamma\omega)^2}\ . \tag{5}$$

For $\omega_0=36\ \mathrm{cm}^{-1}$, $2\Delta=23\ \mathrm{cm}^{-1}$, $g^2\rho=0.1\hbar\omega_0=3.6\ \mathrm{cm}^{-1}$, and $2\gamma=20\ \mathrm{cm}^{-1}$ Fig. 7 shows the theoretical spectral function which should be compared to the A symmetry experimental result.[11] For this "bare" gap value of 23 cm^{-1}, the theoretical CDW peak is centered around 40 cm^{-1} and gap mode peaks at 18.5 cm^{-1}. This curve is very similar to the result obtained for inhomgeneous broadening in Ref. 2. Using a "bare" gap value of 18 cm^{-1} for the E spectrum and the same coupling constant of $0.1\hbar\omega_0$, Fig. 8 was obtained for the theoretical E spectrum. This curve compares fairly well to the experimental result.[11]

Thus assuming the same $g^2\rho$ coupling constant value for the A and E symmetries we obtain a symmetry dependent "bare" BCS energy gap of

$$2\Delta_E=18\ \mathrm{cm}^{-1}\ ,$$

and

$$2\Delta_A=23\ \mathrm{cm}^{-1}\ .$$

On the other hand if one assumes the gap is symmetry independent the observed difference in gap mode frequencies implies that the coupling strength will be different for the A and E modes. In particular $\langle g^2\rho\rangle_E>\langle g^2\rho\rangle_A$.

These results highlight the advantages of the technique of Raman scattering. The good energy resolution enables one to measure such small anisotropies. This is not possible by standard tunneling and infrared techniques.

Figures 9 and 10 show the result of increasing the lifetime broadening of the CDW phonon. The theoretical curves predict almost no shift in the posi-

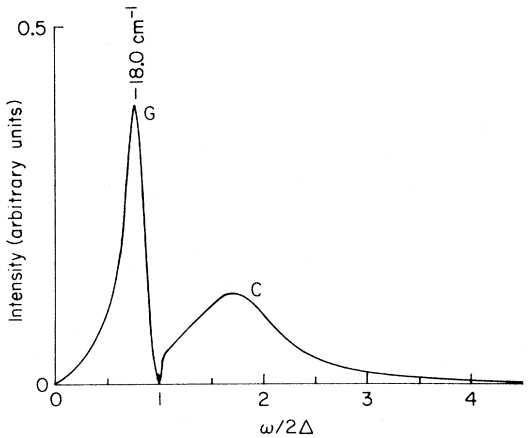

FIG. 7. Effect of lifetime broadening of CDW phonon. The following parameters were used for the A spectrum, $\omega_0=36\ \mathrm{cm}^{-1}$, $2\Delta=23\ \mathrm{cm}^{-1}$, $g^2\rho=0.1\hbar\omega_0=3.6\ \mathrm{cm}^{-1}$, and $2\gamma=20\ \mathrm{cm}^{-1}$. G: "gap" mode; C: CDW mode.

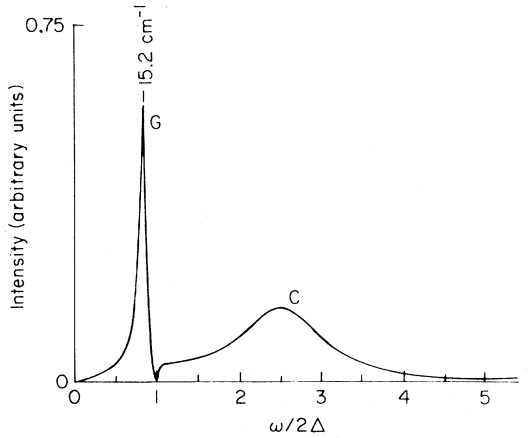

FIG. 8. Effect of lifetime broadening of CDW phonon. The following parameters were used for the E spectrum. $\omega_0=44\ \mathrm{cm}^{-1}$, $2\Delta=18\ \mathrm{cm}^{-1}$, $g^2\rho=0.1\hbar\omega_0=4.4\ \mathrm{cm}^{-1}$, $2\gamma=20\ \mathrm{cm}^{-1}$. G: "gap" model; C: CDW mode.

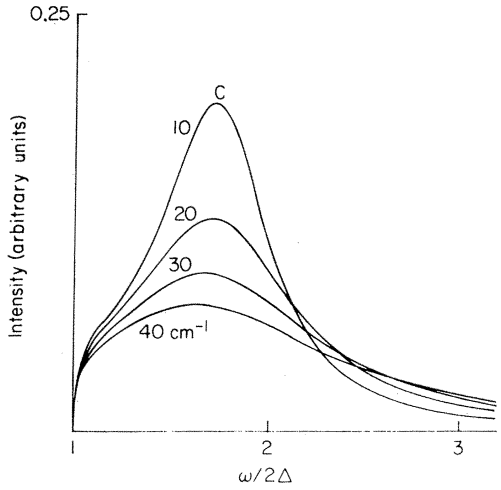

FIG. 9. Effect of increasing the lifetime broadening of the CDW phonon.

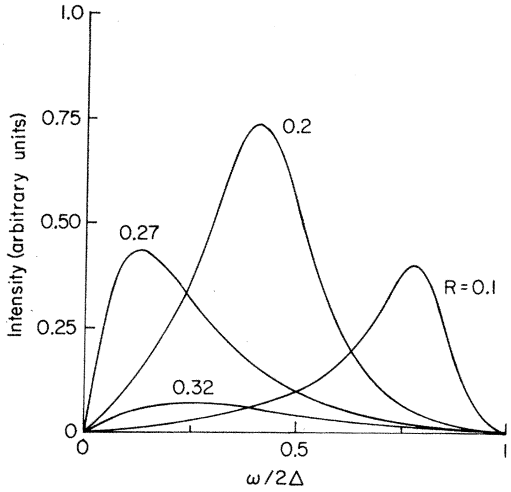

FIG. 11. Effect of increasing coupling strength between CDW phonon and superconducting electrons. Curves show effect on new gap mode for values of $g^2\rho(0)/\hbar\omega_0 = R = 0.1$, 0.2, 0.27, and 0.32.

tion of the peaks, though the line shape of the new gap modes change. A more general, frequency-dependent coupling constant has to be considered for a detailed analysis.

C. Coupling-strength effects

The effect of increasing the coupling strength between the phonon and the gap peaks is shown in Figs. 11 and 12. One would expect the gap modes to soften as $g^2\rho$ is increased and if the coupling to the electrons is strong enough the bound-state frequency should become imaginary. This results in the crystal becoming unstable against spontaneous lattice distortions, i.e., a phase transformation should occur. This, however, is not seen in Fig. 11 because the gap mode becomes overdamped. As the coupling increases from 0.1 to about $0.25\hbar\omega_0$ the peak softens and gains intensity. On further increasing the coupling beyond this value, the intensity begins to drop and the peak (not the actual gap mode frequency) is seen to actually harden. On increasing the coupling, the CDW phonon is seen to become stiffer and its integrated intensity decreases (see Fig. 12).

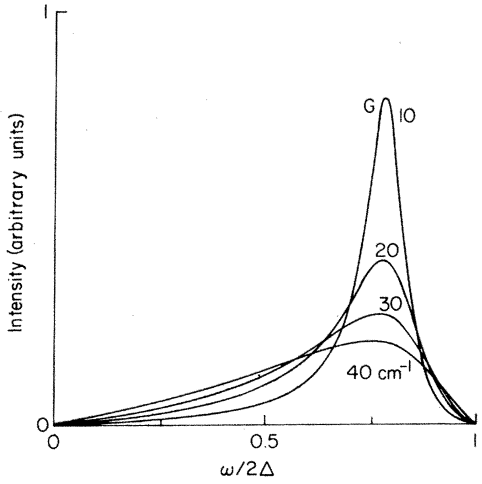

FIG. 10. Effect of increasing lifetime broadening of CDW C on new mode G.

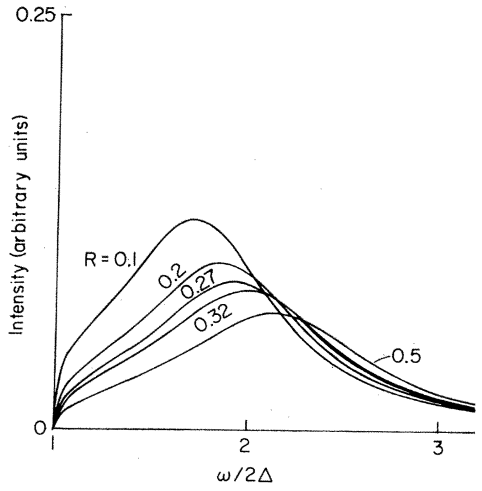

FIG. 12. Effect of increasing coupling strength between CDW phonon C and superconducting electrons. Curves show effect on C for values of $g^2\rho(0)/\hbar\omega_0 = R = 0.1$, 0.2, 0.27, and 0.32, and 0.5.

An exact calculation of the coupling strength in our case would be complicated by the rather complex Fermi surface in $2H$-$NbSe_2$. Moreover, for charge-density-wave phonons, the Fermi surface that is most important depends on the amount of "nesting." This is not well known.[12] The present theory breaks down for coupling strengths $g^2\rho(0)$ greater than $0.25\hbar\omega_0$, i.e., $\simeq 10$ cm^{-1}, for the following reason: The theory assumes a weakly coupled superconductor where $[g^2\rho(0)]/(\hbar\omega_0) = R \approx \frac{1}{8}$ to $\frac{1}{4}$. {Pb and Hg, which are strongly coupled superconductors, have $[g^2\rho(0)]/(\hbar\omega_0)$ greater than 1.}

D. Effect of magnetic fields

$2H$-$NbSe_2$ is a highly anisotropic material. The penetration depths λ and coherence lengths ξ have different values parallel and perpendicular to the layers. These values are reproduced below from Ref. 6

$$\xi_{\parallel} = 77 \text{ Å}, \quad \xi_{\perp} = 23 \text{ Å} ,$$
$$\lambda_{\parallel} = 690 \text{ Å}, \quad \lambda_{\perp} = 2300 \text{ Å} .$$

Due to the metallic nature of the samples, the skin depth δ in these samples is only 300 Å. Comparing with the values of λ, we see that $\lambda_{\parallel,\perp} > \delta$. Hence to some extent, in light-scattering experiments in a magnetic field the samples may behave as thin films.

$2H$-$NbSe_2$ which is also a type-II superconductor exhibits the characteristic vortex regime. In this phase, the order parameter will not be a constant but vary spatially. As the external field increases, the density of vortices increases until at H_{c2} the sample becomes normal. Type II materials behave differently in external fields depending on whether $l/\xi >< 1$ where l is the electron mean free path. Trey *et al.*,[6] in their measurements of the temperature and angular dependence of H_{c2} find that due to the strong anisotropy of the Fermi surface, experimentally, $2H$-$NbSe_2$ does not fall clearly into either category.

The effect of magnetic impurities on an electronic system has been treated by Skalski *et al.*[13] By considering a complex gap $\tilde{\Delta}$ and complex frequency $\tilde{\omega}$ to take account of the magnetic effects, they calculate the self-energy of the system.

We extend this concept of a complex gap to explain our data in a magnetic field and replace Δ by $\tilde{\Delta} = \Delta + i\Gamma$. The magnetic field effects are introduced through Γ. We have chosen the simplest form for Γ—it being frequency independent. Further, in Eq. (1) we approximate $\sum_K$ by $\rho(0)\int d\xi_K$ where $\rho(0)$ is the density of states at the Fermi surface. Thus

$$\Pi(0,\omega) = g^2\rho(0)\tilde{\Delta}^2 \times \int_{-\infty}^{\infty} \frac{d\xi}{(\tilde{\Delta}^2+\xi^2)^{1/2}} \left[\xi^2 + \tilde{\Delta}^2 - \frac{\omega^2}{4}\right]^{-1} . \quad (6)$$

We again calculate $\Pi(0,\omega)$ in the two regions $\omega > 2\Delta$ and $\omega < 2\Delta$ and obtain the spectral function from Eqs. (2) and (3).

1. $\omega > 2\Delta$

$$\Pi(0,\omega) = g^2\rho(0)\tilde{\Delta}^2 I$$

with

$$I = \int_{-\infty}^{\infty} \frac{dZ}{(\tilde{\Delta}^2+Z^2)^{1/2}} \frac{1}{(Z-Z_0)(Z+Z_0)}$$

and

$$Z_0^2 = \left[\frac{\omega^2}{4} - \tilde{\Delta}^2\right] .$$

I has two first order poles at $\pm Z_0$ and branch cuts at $\pm i\tilde{\Delta}$. By carrying out the integral for I, we have

$$I = \frac{2\pi i}{\omega Z_0} - \frac{2}{\omega Z_0} \ln\left[\frac{\omega - 2Z_0}{\omega + 2Z_0}\right] .$$

Writing $Z_0 = re^{i\phi}$ gives

$$I = \frac{2e^{-i\phi}}{\omega r}\left\{i\left[\pi - \tan^{-1}\left[\frac{2\omega r\sin\phi}{4r^2-\omega^2}\right]\right] + \frac{1}{2}\ln\left[\frac{\omega^2+4\omega r\cos\phi+4r^2}{\omega_2-4\omega r\cos\phi+4r^2}\right]\right\} .$$

Thus defining

$$C = \pi - \tan^{-1}\left[\frac{2\omega r\sin\phi}{4r^2-\omega^2}\right] ,$$

$$D = \left[\frac{\omega^2+4\omega r\cos\phi+4r^2}{\omega^2-4\omega r\cos\phi+4r^2}\right] ,$$

$$F' = \mathrm{Re}I = \frac{2}{\omega r}\left(\tfrac{1}{2}\cos\phi\ln D + C\sin\phi\right) ,$$

$$E' = \mathrm{Im}I = \frac{2}{\omega r}\left(C\cos\phi - \tfrac{1}{2}\sin\phi\ln D\right) ,$$

where

$$\phi = \tfrac{1}{2}\tan^{-1}\left[\frac{-2\Delta\Gamma}{\omega^2/4 - \Delta^2 + \Gamma^2}\right] ,$$

then

$$\Pi(0,\omega) = g^2\rho(0)\tilde{\Delta}^2(F' + iE') ,$$

i.e.,

$$\Pi(0,\omega) = g^2p(0)(F + iE) ,$$

where

$$F = [F'(\Delta^2 - \Gamma^2) - 2\Delta\Gamma E']$$

and

$$E=[E'(\Delta^2-\Gamma^2)+2\Delta\Gamma F'] \ .$$

Thus, the spectral function given by Eq. (3) is

$$S(\omega)=\frac{4\omega_0[2\gamma\omega+2\omega_0 E]}{(\omega^2-\omega_0^2-2\omega_0 F^2)+(2\gamma\omega+2\omega_0 E)^2} \ . \quad (7)$$

2. $\omega < 2\Delta$

For frequencies less than 2Δ, C, D, E', and F' are replaced by

$$C=+\left[-\pi+\tan^{-1}\left(\frac{2r\cos\phi}{\omega-2r\sin\phi}\right)+\tan^{-1}\left(\frac{2r\cos\phi}{\omega+2r\sin\phi}\right)\right] , \quad (8)$$

$$D=\frac{\omega^2+4\omega r\sin\phi+4r^2}{\omega^2-4\omega r\sin\phi+4r^2} \ , \quad (9)$$

$$E'=\frac{2}{\omega r}(-C\sin\phi+\tfrac{1}{2}\cos\phi\ln D) \ , \quad (10)$$

$$F'=\frac{2}{\omega r}(C\cos\phi+\tfrac{1}{2}\sin\phi\ln D) \ , \quad (11)$$

and

$$\phi=\tfrac{1}{2}\tan^{-1}\left(\frac{2\Delta\Gamma}{\Delta^2-\Gamma^2-\omega^2/4}\right) \ . \quad (12)$$

Again, $S(\omega)$ is given by Eq. (7).

Figure 13 shows the result of plotting Eq. (7) in regions $\omega > 2\Delta$ and $\omega < 2\Delta$. The effect of increasing Γ, the imaginary part of the energy gap is also shown.

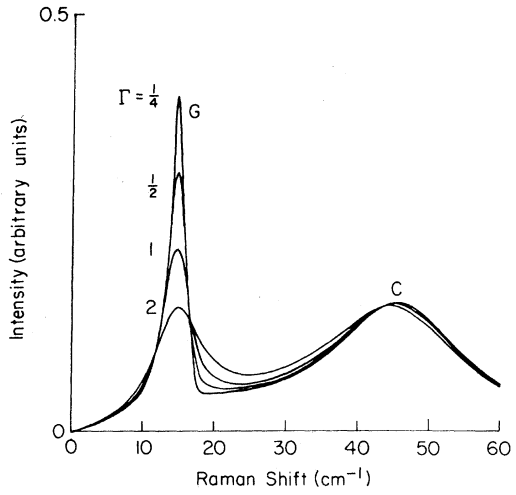

FIG. 13. Effect of increasing Γ, the imaginary part of the gap. The parameters used were $\omega_0=44$ cm^{-1}, $g^2\rho=0.1\hbar\omega_0=4.4$ cm^{-1}, $2\Delta=18$ cm^{-1}. The parameters were chosen to approach the E spectrum results of Fig. 6. $\Gamma=\frac{1}{4}$, $\frac{1}{2}$, 1, and 2 cm^{-1}.

The parameters used in these graphs are

$$\omega_0=44 \text{ cm}^{-1} \ ,$$

$$g^2\rho=0.1\hbar\omega_0=4.4 \text{ cm}^{-1} \ ,$$

$$\Delta=9 \text{ cm}^{-1} \ ,$$

and Γ has values of $\frac{1}{4}$, $\frac{1}{2}$, 1, and 2 cm^{-1}. This set of values was chosen for the parameters to approach the E spectrum results. The theoretical curves have the following features: (1) The new gap modes are seen to decrease in strength rapidly when Γ increases. There is no shift in the peak position. This agrees closely with the experimental results (Fig. 6). (2) The discontinuity at $\omega=2\Delta$ which is present when Δ is real has been removed. (3) When Γ gets larger, the CDW phonon is seen to soften by a very small amount.

The Raman intensity lost at the gap modes as Γ increases is apparently redistributed between approximately 18 and 35 cm^{-1}. The shift in the positions of C, which is rather small, is not apparent from the experimental results. This could be due to the resolution used in the experiment and the limited signal-to-noise ratio.

Figure 14 shows similar theoretical curves for the A spectrum with $\Delta=11.5$ cm^{-1}. Theoretically, the peak height of the CDW mode in the A spectrum is smaller than the mode G. This is not so experimentally. A more detailed frequency-dependent coupling strength is probably required to cause experiment and theory to agree on this aspect. When $\Gamma=0$, we get back the results obtained for real Δ.

We thus see that the concept of an imaginary gap qualitatively explains most of the experimental results. Considering the simplicity of the model

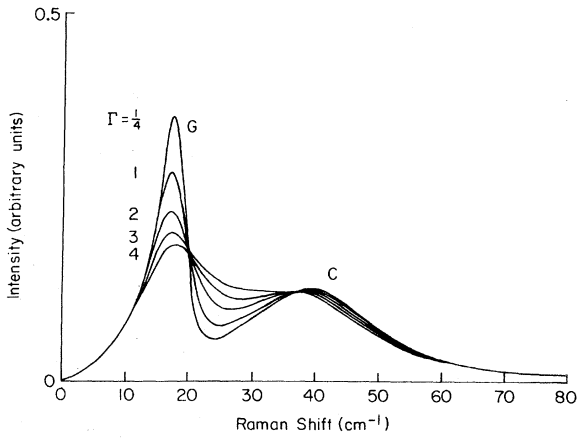

FIG. 14. Effect of increasing Γ, the imaginary part of the gap. The parameters used were $\omega_0=36$ cm^{-1}, $g^2\rho=0.1\hbar\omega_0=3.6$ cm^{-1}, $2\Delta=23$ cm^{-1}. The parameters were chosen to approach the A spectrum results of Fig. 2. $\Gamma=\frac{1}{4}$, 1, 2, 3, and 4 cm^{-1}.

used, the agreement between theory and experiment is good. In conclusion, the experiments and theory clearly show the direct coupling between the CDW phonon and superconductivity electrons. The complex gap model explains qualitatively the behavior of the Raman modes in a magnetic field. Moreover, the discontinuous behavior of the theoretical curve at 2Δ when Δ is real, is removed when a small imaginary part is added to the gap. This suggests the possibility of a spin-dependent coupling between the CDW and superconducting electrons.

Improvements to the theory presented are certainly possible. A more detailed theory should also consider the properties of the CDW to a greater extent. For instance since only electrons near a "nested" Fermi surface are affected by a CDW, the Fermi surface anisotropy is important. This would result in a more complex coupling between the electrons and phonon than that presented. Hence both the CDW and superconducting interactions should be included in the Hamiltonian.

Improvements in the theory for the results in a magnetic field can also be made. We have considered the simplest case of $\tilde{\Delta} = \Delta + i\Gamma$, where Γ is frequency independent. By considering proper frequency dependence as suggested in Ref. 13 better agreements in the line shapes may perhaps be obtained.

ACKNOWLEDGMENTS

We thank S. F. Meyer, F. J. DiSalvo, R. V. Coleman, and R. F. Frindt for providing crystals and J. P. Wolfe for the use of a cryostat for the magnetic-field-dependent studies. Thanks go to W. L. McMillan and John Bardeen for theoretical discussions, and especially, to L. M. Falicov for may conversations and for his patient explanation of the theory of Ref. 2. This work was supported by the National Science Foundation under the MRL Grant No. DMR-77-23999.

---

*Present address: Max-Planck-Institut für Festkorperforschung, Heisenbergstrasse 1, 7000 Stuttgart 80, West Germany.

[1]R. Sooryakumar and M. V. Klein, Phys. Rev. Lett. 45, 660 (1980).

[2]C. A. Balseiro and L. Falicov, Phys. Rev. Lett. 45, 662 (1980).

[3]R. Sooryakumar, M. V. Klein, and R. F. Frindt, Phys. Rev. B 23, 3222 (1981) (following paper).

[4]D. G. Bruns, Ph.D. dissertation (University of Illinois, Urbana, Illinois, 1979) (unpublished).

[5]Provided by F. J. DiSalvo of Bell Laboratories. See Ref. 3 for further results from this sample in the absence of a magnetic field.

[6]P. de Trey, Suso Gygax, and J. P. Jan, J. Low Temp. Phys. 11, 421 (1973).

[7]This is essentially the Thomas-Reiche-Kuhn sum rule for the oscillator strength associated with the operator u.

[8]T. J. Greytak and J. Yan, Phys. Rev. Lett. 22, 987 (1967).

[9]J. A. Holy, Ph.D. dissertation (University of Illinois, Urbana, Illinois, 1977) (unpublished).

[10]R. Sooryakumar, Ph.D. dissertation (University of Illinois, Urbana, Illinois, 1980) (unpublished).

[11]The results in the absence of magnetic fields from $2H$-$NbSe_2$ samples of diverse quality are presented in Ref. 3. Results from sample M in this reference show a well-defined strong CDW phonon.

[12]G. K. Bristow, T. R. Finlayson, and T. F. Smith, Phys. Status Solidi (b) 82, K81 (1977).

[13]S. Skalski, O. Betbeder-Matibet, and P. R. Weiss, Phys. Rev. 136, A1500 (1964).